CLEO's Impact on CKM

P.D. Rubin
Department of Physics & Astronomy, MSN 3F3
George Mason University
Fairfax, VA 22030 USA
For the CLEO-c Collaboration

In the six-quark Standard Model, flavor changing due to the weak force is described by a unitary transformation represented by the 3×3 matrix, known as the Cabibbo-Kobayashi-Maskawa (CKM) matrix. The elements of this matrix, constrained theoretically by unitarity, must be determined experimentally. By investigating e^+e^- collisions around the charm-quark threshold, the CLEO-c experiment has gleaned results relevant to the elements V_{cs}, V_{cd}, V_{ub}, and V_{cb} from semi-leptonic, leptonic, and multi-hadronic decays of D mesons. We present these results.

1 Introduction

The CLEO-c program of running the $e^+ - e^-$ collider CESR just above $D_{(s)}\bar{D}^{(*)}_{(s)}$ threshold has yielded a number of results which increase, or can increase, the precision of our knowledge o the Cabibbo-Kobayashi-Maskawa mixing matrix elements.

Measurements of $D \to (K/\pi)e\nu$ rates lead directly to measurements of the elements $|V_{cd}$ and $|V_{cs}|$ and afford the opportunity to determine form factors:

$$\frac{d\Gamma(D \to (K/\pi)e\nu)}{dq^2} = \frac{G_F^2 P_{K/\pi}^3}{24\pi^3}|V_{cs(cd)}|^2|f_+(q^2)|^2. \quad (1$$

Comparison of such determinations with LQCD calculations may build confidence in the appli cation of the latter to measurements of $|V_{ub}|$, in which the $b \to u$ rate is too small to measure the form factor.

Similarly, measuring the leptonic decay $D_s^+ \to \ell^+\nu$ allows a determination of the decay

constant $f_{D_s^+}$:

$$\Gamma(D_s^+ \to \ell^+\nu) = \frac{G_F^2 m_{D_s^+} m_\ell^2 \left(1 - \frac{m_\ell^2}{m_{D_s^+}^2}\right)^2}{8\pi} |V_{cs}|^2 f_{D_s^+}^2. \quad (2)$$

This can be compared to LQCD predictions. LQCD also predicts f_B and the ratio f_{B_s}/f_B, which values are needed to pull out $|V_{ub}|$ from B leptonic decays, $|V_{td}|$ from $B - \bar{B}$ mixing, and $|V_{ts}|$ from $B_s - \bar{B}_s$ mixing.

The mixing matrix is unitary, and this leads to relationships between its (complex) elements. One such relationship,

$$V_{ud}V_{ub}^* + V_{cd}V_{cb}^* + V_{td}V_{tb}^* = 0, \quad (3)$$

can be visualized as a triangle in the complex plane. The interior angles of this triangle, two of which, $\alpha \equiv \phi_1$ and $\beta \equiv \phi_2$, are well measured, give the relative phases between pairs of matrix elements. The third angle, $\gamma \equiv \phi_3 \equiv \arg\left(-\frac{V_{ud}V_{ub}^*}{V_{cd}V_{cb}^*}\right)$, the phase of V_{ub} relative to V_{cb}, is not yet sufficiently well-measured to confirm relationship (3). It is accessible as a result of interference between $b \to c$ and $b \to u$ transitions, and, through such loop diagrams, sensitive to physics beyond the Standard Model. One obvious approach to measuring γ is with the decays $B^\pm \to \tilde{D}^0 K^\pm$, where $\tilde{D}^0$ indicates that the $B^\pm$ can decay to either D^0 or $\bar{D}^0$:

$$\mathcal{A}(B^\pm \to \tilde{D}^0 K^\pm) \propto \mathcal{A}_{D^0} + r_B e^{i(\delta_B \pm \gamma)} \mathcal{A}_{\bar{D}^0}, \quad (4)$$

where r_B is the relative rate for $B^\pm$ going to D^0 or $\bar{D}^0$. The D^0 and $\bar{D}^0$ can decay into the same final state of $K_{L/S}(K/\pi)n\pi$, where n can be 0, 1,.... For the case of $\tilde{D}^0 \to K_{L/S}\pi\pi$ there is a strong phase difference between the D^0 and $\bar{D}^0$ transitions, and the uncertainty of its value, presently 7% – 9%, will limit the precision of the γ measurement. For $K^+\pi^-$ there is a strong phase:

$$\Gamma(B^\pm \to (K^+\pi^-)_{\tilde{D}^0} K^\pm) \propto r_B^2 + (r_D^{K\pi})^2 + 2r_B r_D^{K\pi} \cos(\delta_B + \boldsymbol{\delta_D^{K\pi}} - \gamma), \quad (5)$$

and for $K^+\pi^-\pi^-\pi^+$ there is a strong phase and a coherence factor:

$$\Gamma(B^\pm \to (K^+\pi^-\pi^-\pi^+)_{\tilde{D}^0} K^\pm) \propto r_B^2 + (r_D^{K3\pi})^2 + 2\mathbf{R_D^{K3\pi}} r_B r_D^{K3\pi} \cos(\delta_B + \boldsymbol{\delta_D^{K3\pi}} - \gamma), \quad (6)$$

2 Data

The CLEO investigations around charm threshold were carried out at Cornell University's CESR, which was built to run at Υ energies. To run at lower energies with reasonable luminosities required the insertion into the ring of a series of wiggler magnets, as well as new beamline optics (particularly around the CLEO detector), and upgraded beam monitoring tools. In addition, the silicon vertex array of the CLEO-III detector was replaced by an inner wire chamber, and the solenoid field was lowered from 1.5 to 1 Tesla for the typically lower momentum tracks produced at the lower collision energies.

During the CLEO-c era, then, CESR primarily operated just above the $\psi(3770) \to D\bar{D}$ threshold, where some 818 pb^{-1} of integrated luminosity were collected, and near the $D_s\bar{D}_s^*$ threshold, E_cm = 4170 MeV, where about 600 pb^{-1} of integrated luminosity were collected. This latter energy choice was based on an energy scan above the $D_s\bar{D}_s$ threshold which found it to yield the highest number of D_s mesons.

CESR ceased its particle physics service in March, 2008.

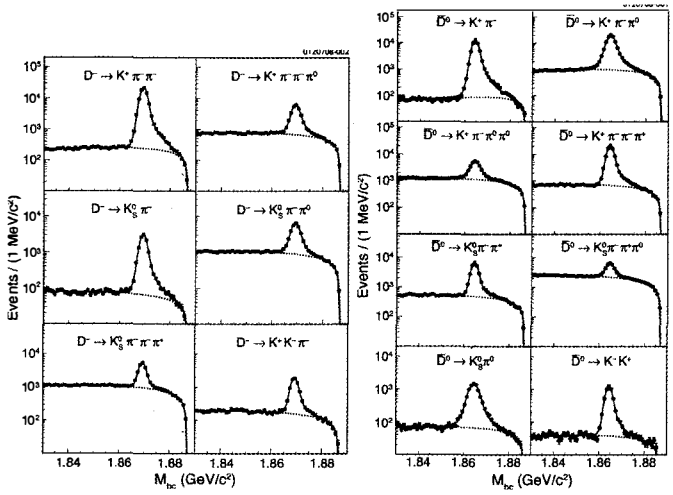

Figure 1: (left)Charged tagging modes; (right)Neutral tagging modes. Shown are the projections on the beam constrained mass ($M_{bc} \equiv \sqrt{E^2_{\rm beam} - |\vec{p}_D|^2}$) axis after a mode-specific cut on energy difference ($\Delta E \equiv E_D - E_{\rm beam}$ Estimated background is shown by a dashed curve.

2.1 Tagging

The primary advantages of running at these thresholds are that the production of two-bod states is optimized and the cross-sections are relatively high. Given these and the good lumi nosities provided by CESR and the hermiticity of the CLEO detector, the full reconstruction c at least one member of the pair via one of several dominant decay modes was highly efficient Tagging of an event in this way reduces backgrounds and kinematic ambiguity when determinin what happens to the other member.

2.2 Coherence

The $\psi(3770)$ is in a $= -1$ state, so the $D^0\bar{D}^0$ pair is correlated quantum mechanically Thus, tags can give not only flavor and channel information, but also P state informatior This increases the analyzing power of Dalitz plots by permitting model-independent access t both the magnitude and phase of decay amplitudes. Ultimately, this can reduce systematic o model-dependent uncertainties of analyses, such as measurements of unitarity triangle angles.

3 Semileptonic Branching Ratios and Form Factors, and $|V_{cs}|$ and $|V_{cd}|$

3.1 Tagged Analysis

For the tagged Semileptonic analysis, six charged modes and eight neutral modes were used fo the tagging [see Figure 1]. Note that the ordinate is logarithmic in all cases.

Once the event is tagged as being $D\bar{D}$, and a kaon or pion and an electron are identifiec a quantity, $U \equiv E_{\rm miss} - |\vec{p}_{\rm miss}|$, related to missing mass squared, is calculated [see Figure 2 Note that the quantities involved have been corrected for the ~ 3 mrad crossing angle at th interaction point. $U = 0$ indicates what is missing is a neutrino, and therefore the decay wa semileptonic.

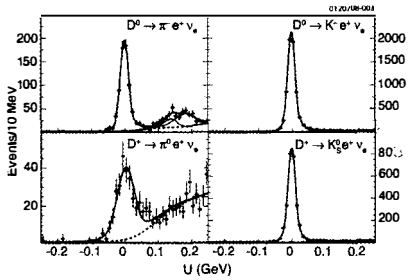

gure 2: $U \equiv E_{\rm miss} - |\vec{p}_{\rm miss}|$ for tagged events with, additionally, a kaon or pion and an electron. $\sigma_U \approx 12(24)$ MeV for events with a $K^{\pm}$, $\pi^{\pm}$, or K^0_S (π^0).

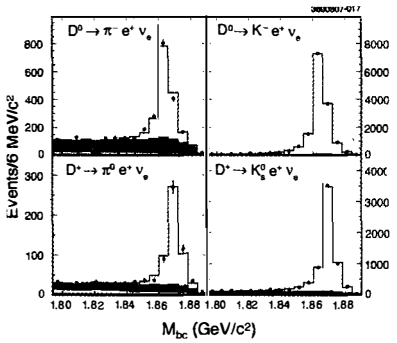

Figure 3: Beam-constrained mass from untagged semileptonic analysis.

2 *Untagged Analysis*

the untagged analysis, all information available is used to reconstruct a neutrino 4-vector, nich is combined with those of a kaon or pion and an electron. The resulting energy is required be consistent with the beam energy, and the beam-constrained mass is computed [see Figure 3]. ne event-finding efficiency is higher for this method than for the tagged analysis, but both the ckground and systematic uncertainties are larger.

3 *Branching Fractions*

ble 1 gives the branching fractions (in %) from 281 pb^{-1} of data (the full data-set result is ming soon). Notice that the resolutions of the two analysis approaches are comparable.

ble 1: Branching fractions (in %) from the two $D \to (K/\pi)e\nu$ analyses of the first 281 pb^{-1} of data. The t uncertainty is statistical, the second combines systematical and theoretical uncertainties. Averages take into account correlations.

	Tagged	Untagged	Average
$\pi^- e^+ \nu_e$	0.308 (13) (4)	0.299 (11) (9)	0.304 (11) (5)
$\pi^0 e^+ \nu_e$	0.379 (27) (23)	0.373 (22) (13)	0.378 (20) (12)
$K^- e^+ \nu_e$	3.60 (5) (5)	3.56 (3) (9)	3.60 (3) (6)
$K^0 e^+ \nu_e$	8.87 (17) (21)	8.53 (13) (23)	8.69 (12) (19)

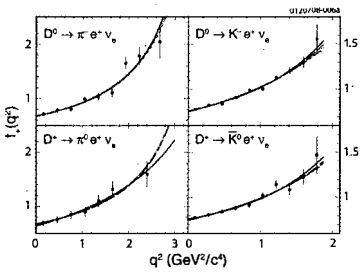

Figure 4: Differential decay rate as a function of q^2. Curves are fits of the models to the data.

3.4 Form Factors

The rate of the decay $D \to (K/\pi)e\nu$ is related to the product of the mixing matrix element an a q^2-dependent form factor, $f_+(q^2)$ [see Equation (1)]. Measuring this rate and fixing the valu of the matrix element, one can calculate $f_+(q^2)$ as a function of q^2 [see Figure 4]. Fits are t three models [1]

$$\text{Simple Pole}: \quad f_+(q^2) = \frac{f_+(0)}{1 - \frac{q^2}{M^2_{\text{pole}}}} \tag{7}$$

$$\text{Modified Pole}: \quad f_+(q^2) = \frac{f_+(0)}{\left(1 - \frac{q^2}{M^2_{\text{pole}}}\right)\left(1 - \alpha\frac{q^2}{M^2_{\text{pole}}}\right)} \tag{8}$$

$$\text{Series Expansion}: \quad f_+(q^2) = \frac{a_0}{P(q^2)\phi(q^2,t_0)}\left(1 + \sum_k a_k(t_0)z(q^2,t_0)^k\right) \tag{9}$$

In fact, these data are unable to distingish between the models, when all parameters are allowe to float. However, the best fit to the pole models requires an unphysical M_{pole}.

3.5 $|V_{cd}|$ and $|V_{cs}|$

Fixing, instead, $f_+(q^2)$, in this case to a value calculated by LQCD, allows the mixing matri elements to be calculated:

$$|V_{cd}| = 0.233 \pm 0.008_{\text{stat}} \pm 0.003_{\text{syst}} \pm 0.023_{\text{theo}} \tag{10}$$

$$|V_{cs}| = 1.019 \pm 0.010_{\text{stat}} \pm 0.007_{\text{syst}} \pm 0.106_{\text{theo}} \tag{11}$$

The first of these is the best measurement from semileptonic D-meson decays, and the secon is the best determination regardless of technique. [2,3,4]

4 $f_{D_s^+}$ from $D_s^+ \to \ell^+\nu_\ell$

As Equation (2) shows, the form factor $f_{D_s^+}$ can be determined from the rate of $D_s^+ \to \ell^+\nu_\ell$ Two approaches were taken, a generic lepton measurement and a specific τ channel.

4.1 $D_s^+ \to \ell^+\nu_\ell$

Eight D_s^- tag modes were used: $K^+K^-\pi^-$, $K_S^0K^-$, $\eta\pi^-$, $\eta'\pi^-$, $K_S^+K^-\pi^-\pi^0$, $\pi^+\pi^-\pi^-$, $K^{*0}K^{*-}$ and $\eta'\rho^-$. Recall that the collision energy producing the D_s mesons was just above $D_s\bar{D}_s^*$, s that, in addition to the D_s^+ partner to the tag, there will also be at least one high energy photo

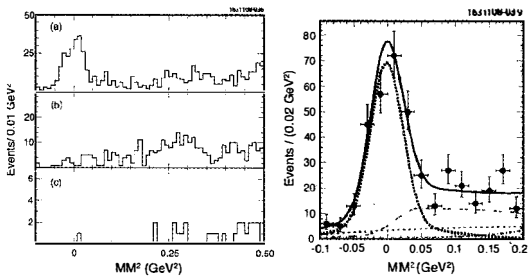

gure 5: Missing mass squared [see Equation (13)]. On the left, (a) events with a non-tag track depositing < 300 eV in the calorimeter; (b) events with a track depositing > 300 MeV but not satisfying electron identification iteria; and (c) events with an identified electron. On the right, data from cases (a) and (b) combined (black ots); the solid blue curve sums $\mu^+\nu_\mu$ MC (black dot curve), $\tau^+\nu_\tau$, $\tau^+ \to \pi^+\bar{\nu}_\tau$ MC (purple double dash-dot curve), D_s^+ sidebands [see Equation (12)] (red dash curve), and other D_s^+ channels (green dot dash curve).

the final state. Combining a candidate photon with the tag allows the computation of a issing mass squared, whose signal value would be around $m^2_{D_s}$:

$$MM^{*2} = (E_{CM} - E_{D_s^-} - E_\gamma)^2 - (-\vec{p}_{D_s^-} - \vec{p}_\gamma)^2 \tag{12}$$

Events selected in the signal region of this quantity are checked for the presence of at least ne additional charged track. Assuming it to be a muon, another missing mass squared quantity calculated:

$$MM^2 = (E_{CM} - E_{D_s^-} - E_\gamma - E_\mu)^2 - (-\vec{p}_{D_s^-} - \vec{p}_\gamma - \vec{p}_\mu)^2 \tag{13}$$

the track deposits less than 300 MeV in the calorimeter, it is likely a muon. If it deposits ore than 300 MeV, it is likely a pion from a tau decay or an electron (certain characteristics, ke E/p, allow the distinction to be made). The three possibilities for Equation (13) are shown the left plot of Figure 5, and the combination of the first two possibilities is shown in the ght plot.

2 $D_s^+ \to \tau^+\nu_\tau$, $\tau^+ \to e^+\nu_e\bar{\nu}_\tau$

or this analysis, $D_s^- \to \phi\pi^-$, $D_s^- \to K^{*0}K^-$, and $D_s^- \to K_S^0K^-$, were the only tags. If an ectron was identified with the good tag, extra energy in the calormeter, presumably from the $_s^* \to (\gamma/\pi^0)D_s$, was plotted, and the signal region was defined as $E_{\rm signal}$ o 400 MeV. The yield as the count in the signal region after tag sideband subtraction.

3 *Branching Fractions and* $f_{D_s^+}$

he results of these searches are shown in Table 2. A comparison with selected predictions

Table 2: Branching fractions and $f_{D_s^+}$ from $D_s^+ \to \ell^+\nu_\ell$.

Mode	BF [%]	$f_{D_s^+}$ [MeV]
(1) $\mu\nu$	$0.565 \pm 0.045 \pm 0.017$	$257.3 \pm 10.3 \pm 3.9$
(2) $\tau\nu$, $\tau \to \pi\nu$	$6.42 \pm 0.81 \pm 0.18$	$278.7 \pm 17.1 \pm 3.8$
(3) $\mu\nu$ (eff) [$\tau\nu/\mu\nu$ fixed to SM ratio]	$0.591 \pm 0.037 \pm 0.018$	$263.3 \pm 8.2 \pm 5.2$
(4) $\tau\nu$, $\tau \to e\nu\nu$	$5.30 \pm 0.47 \pm 0.22$	$252.5 \pm 11.1 \pm 5.2$
CLEO average from (3) and (4)		$259.5 \pm 6.6 \pm 3.1$

long with a similar comparison for f_{D^+}) can be seen in Figure 6. [5,6,7,8,9]

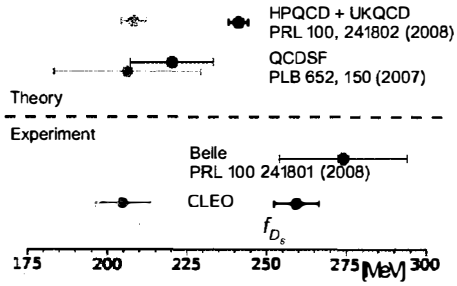

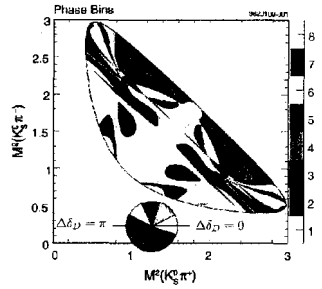

Figure 7: Binning for Dalitz analysis of $D \to K_{S/L}\pi\pi$

5 Reducing γ/ϕ_3 Measurement Uncertainties

Uncertainties from the strong phase in D-meson decay channels contribute as much as 10° to t uncertainty of γ/ϕ_3. Sensitive studies of these channels can reduce this uncertainty significant CLEO has taken two approaches to such studies. [13,14,15,16]

5.1 Strong Phase Difference in $D \to K_{S/L}\pi\pi$

The charged B-meson can decay to $\tilde{D}K^{\pm}$, where $\tilde{D}$ is *either* D^0 *or* $\bar{D}^0$. The D^0 and the $\bar{D}^0$ may, in turn, decay into the same final state, say $K_{S/L}\pi\pi$. The relative rates are sensitive to strong phase difference, $\Delta\delta_{D^0}$, between the two channels. The interefence amplitudes of the can be parameterized in terms of the phase difference through the transcendental functio $\cos[\Delta\delta_{D^0}(x,\ y)]$ and $\sin[\Delta\delta_{D^0}(x,\ y)]$, where $(x,\ y)$ are Dalitz-plot variables, here taken to $(M^2(K_{S/L}\pi^+,\ M^2(K_{S/L}\pi^-)$. The plot itself was divided into an even number of bins, index from $-i$ to i symmetrically around the line $y = x$, so that $x \leftrightarrow y \Leftrightarrow -i \leftrightarrow i$. [10] Furthermore, t bin locations, sizes, and shapes were chosen so as to minimize $\Delta\delta_{D^0}$ variatons within a bin and b population differences [see Figure 7]. [11,12] Because CP tags are sensitive to $\cos[\Delta\delta_{D^0}(x,\ y)]$, wh $D \to K_{S/L}\pi\pi$ tags are sensitive to both $\cos[\Delta\delta_{D^0}(x,\ y)]$ and $\sin[\Delta\delta_{D^0}(x,\ y)]$, the dependen on the functions can be extracted. The results have been estimated to decrease the uncertain on the strong phase difference to no more than 2°.

5.2 The Atwood-Dunietz-Soni Method

Coherent double-tag rates are sensitive to combinations of coherence factors and strong phas [see Equation (6)]. [17] For example, the double-tag rate of $K^{\pm}\pi^{\mp}\pi^-\pi^+$ vs. $K^{\pm}\pi^{\mp}\pi^-\pi^+$ is sensiti

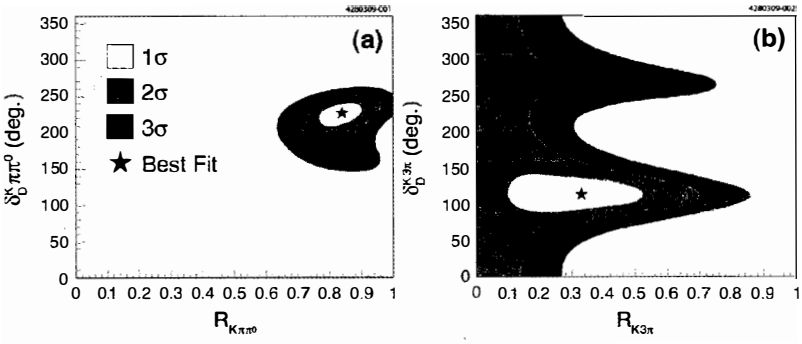

Figure 8: Preliminary values for coherence factors and strong phase.

$(R_D^{K3\pi})^2$, while that of $K^\pm\pi^\mp\pi^-\pi^+$ vs $K^\pm\pi^\mp$ is sensitive to $R_D^{K3\pi}\cos(\delta_D^{K\pi} - \delta_D^{K3\pi})$.

A result for $\delta_D^{K\pi} = (22.5^{+10.5}_{-12.0})^\circ$ was reported in ICHEP08 HFAG. Here we give the preliminary results [see Figure 8]:

$$R_D^{K3\pi} = 0.33^{+0.20}_{-0.23} \quad \delta_D^{K3\pi} = (114^{+20}_{-23})$$
$$R_D^{K\pi\pi^0} = 0.84 \pm 0.7 \quad \delta_D^{K\pi\pi^0} = (227^{+14}_{-17})$$

cknowledgments

nding from the National Science Foundation has supported the author's participation in the LEO-c collaboration and from the Jeffress Memorial Trust supported his conference attendance.

eferences

1. T. Becher and R.J. Hill, *Phys. Lett.* B **633**, 61 (2006).
2. D. Cronin-Hennessy *et al*, *Phys. Rev. Lett.* **100**, 251802 (2008).
3. S. Dobbs *et al*, *Phys. Rev.* D **77**, 112005 (2008).
4. J.Y. Ye *et al*, *Phys. Rev.* D **79**, 052010 (2009).
5. B.A. Dobrescu and A.S. Kronfeld *Phys. Rev. Lett.* **100**, 241802 (2008).
6. QCDSF Collaboration *Phys. Lett.* B **652**, 150 (2007).
7. L. Widhalm *et al*, *Phys. Rev. Lett.* **100**, 241801 (2008).
8. J.P. Alexander *et al*, *Phys. Rev.* D **79**, 052001 (2009).
9. P.U.E. Onyisi *et al*, *Phys. Rev.* D **79**, 052002 (2009).
0. A. Giri *et al*, *Phys. Rev.* D **68**, 054018 (2003).
1. A. Bondar and A. Poluektov *EPJC* **47**, 347 (2006).
2. B. Aubert *et al*, *Phys. Rev. Lett.* **95**, 121802 (2005).
3. J.L. Rosner *et al*, *Phys. Rev. Lett.* **100**, 221801 (2008).
4. D. Asner *et al*, *Phys. Rev.* D **78**, 012001 (2008).
5. R.A. Briere *et al*, submitted to *Phys. Rev.* D, arXiv:0903.1681.
6. N. Lowrey *et al*, submitted to *Phys. Rev. Lett.*, arXiv:0903.4853,
7. D. Atwood, I. Dunietz, and A. Soni, *Phys. Rev. Lett.* **78**, 3257 (1997).